Near-threshold ultraviolet-laser ablation of Kapton film investigated by x-ray photoelectron spectroscopy

D.W. Zeng[a)]
The State Key Laboratory of Plastic Forming Simulation and Mould Technology, Department of Materials Science and Engineering, Huazhong University of Science and Technology, Wuhan (430074), People's Republic of China

K.C. Yung
Department of Industrial and Systems Engineering, The Hong Kong Polytechnic University, Hung Hom, Kowloon, Hong Kong, People's Republic of China

C.S. Xie
The State Key Laboratory of Plastic Forming Simulation and Mould Technology, Department of Materials Science and Engineering, Huazhong University of Science and Technology, Wuhan (430074), People's Republic of China

(Received 9 July 2002; accepted 8 October 2002)

Near-threshold ultraviolet-laser (355 nm) ablation of 125-μm thick Kapton films was investigated in detail using x-ray photoelectron spectroscopy. Different from the irradiation at higher fluences, the contents of the oxygen, amide group, and C–O group on the ablated surface increased with an increase in the pulse number, whereas the carbon contents decreased, although the contents of the nitrogen and the carbonyl group (C = O) decreased slightly. This implied that there was no carbon-rich residue on the ablated surface. Near the ablation threshold, only photolysis of the C–N bond in the imide rings and the diaryl ether group (C–O) took place due to a low surface temperature rise, and the amide structure and many unstable free radical groups were created. Sequentially, the oxidation reaction occurred to stabilize the free radical groups. The decomposition and oxidation mechanism could explain the intriguing changes of the chemical composition and characteristics of the ablated surface. In addition, the content of the C–O group depended on the opposite factors: the thermally induced decomposition of the ether groups and the pyrolysis of the C_{aryl}–C bond. Upon further irradiation, the cumulative heating may induce the breakage of the C_{aryl}–C bond and enhance the oxidation reaction, resulting in an increase of the content of the C–O group.

I. INTRODUCTION

Since ultraviolet (UV) pulsed laser ablation of polymers was first reported,[1,2] it has been studied extensively. These studies clearly show that ablation caused clean etching of polymers with excellent size resolution. Until now, UV pulsed laser ablation of polymers, as a dominant microvia technology, is a routine part in the manufacture of the high-density printed boards and substrates.[3] Despite the large number of experimental and theoretical studies, the mechanisms involved in UV pulsed laser ablation of polymers—photothermal[4–8] versus photochemical[9–12]—are still often controversial. Still other researchers have concluded that photothermal and photochemical decomposition both contribute, with each dominating depending on the ablating conditions and chemical structure of polymers.[13–17] During laser ablation of polymers, the composition and chemical structure of the ablated surface is of potential use for design of UV laser tools for drilling. Srinivasan[12] has repeatedly emphasized the importance of looking into the composition and characteristics of the ablated surface to establish or test the ablation mechanism. By analyzing Raman and infrared characteristics of the ablated surface, Srinivasan[18] and Ortelli[19] have developed possible decomposition paths of the ablated Kapton film. Lippert found that there is graphitic material inside the crater.[20] However, chemical analysis of the ablated surface has not attracted as much interest in the physical aspects of UV laser ablation of polymers.

The analytical method of choice should be sensitive enough for the chemical and structural alterations of the ablated surface and should also be capable of identifying

a)Address all correspondence to this author.
e-mail: davizeng@public.wh.hb.cn

changes in specific groups in the polymer chains. Among various surface sensitive techniques, infrared spectroscopy, especially diffuse reflectance infrared Fourier transform spectroscopy,[19,21] is powerful for analyzing the changes in the specific groups of the ablated surface. Another suitable surface sensitive technique is x-ray photoelectron spectroscopy (XPS), which has been widely used for investigating the changes in the composition and chemical states of the ablated surface.[20,22–26]

Several studies have shown that there are novel ablation behaviors near the threshold. For the purely photothermal mechanism involved in UV pulsed laser ablation of polyimide, the ablated depth Δh near the threshold shows an Arrhenius-type behavior $\Delta h = A\exp(-B/F)$; in contrast, for the purely photochemical mechanism (193 nm ArF-laser), the ablated depth Δh near the threshold can be accurately predicted by Beer's law $\Delta h = \alpha^{-1}\ln(F/F_{th})$.[27–29] Using atomic force microscopy (AFM), Himmelbaur *et al.* systematically investigated the UV-laser-induced surface topology changes in polyimide, and they found that the surface structure near the threshold was evidently different from that at a fluence much higher than the threshold value.[30–32] Nevertheless, there is little research focusing on the composition and chemical characteristics of the polymers ablated by UV pulsed laser near the threshold.[19–20]

Kapton film has been widely applied in microelectronic packaging as a dielectric substrate because of its high thermal stability and good dielectric properties.[33,34] Also, it was usually used as an model material for studying the ablation mechanism.[19,24] In this paper, near threshold laser ablation of Kapton film was carried out using a UV pulsed laser at 355 nm. To ascertain the ablation mechanism, the composition and chemical states of the ablated surface are systematically investigated by XPS and the decomposition path of the Kapton film is discussed in details. This study should lead to a better understanding of the UV-pulsed-laser-drilling behavior of Kapton film.

II. EXPERIMENTAL

Kapton film (125 μm thick) supplied by Dupont (Circleville, OH) was used in this experiment, and its chemical structure is shown in Fig. 1. The experimental method was been reported earlier[13,17,25] and is repeated briefly here. The ablation experiments were carried out in air using a frequency-tripled pulsed Nd:yttrium aluminum garnet (YAG) laser (ESI 5200) (Electro Scientific Industries Inc., Portland, OR) operating at 355 nm with a pulse duration of 60 ns. The beam is Gaussian mode, and its spot size was defined as the position where the laser energy decreases to $1/e^2$ of the peak value. Beam spot size was fixed at 50 μm by adjusting the focus length. The laser ablation was performed in a punch pattern for the measurement of the ablation rate under different fluences ranging from 0.1 to 196 Jcm^{-2}. Also, it was done in a routing pattern at a fixed velocity of 45 mms^{-1} for XPS analysis. The number of pulses varied from 10 to 1000 and the fluence was kept on 0.34 Jcm^{-2} (in the linear region, near ablation threshold). The size of the ablated surface was 2×2 mm^2, much larger than that of the analyzed (typically 0.2 mm in diameter), ensuring that only the irradiated part of the Kapton films was measured.

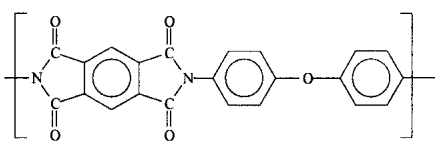

FIG. 1. Chemical structure of Kapton film.

XPS spectra were obtained from the ablated surface by means of a Quantum 2000 spectrometer (Physical Electronics Inc., Eden Prairie, MN) using a nonmonochromatized Al K_σ excitation radiation. During the measurement, the pressure in the working chamber was kept below 5.0×10^{-8} torr. The photoelectron take-off angle with respect to the surface normal was 45°, and the high-resolution spectra were taken at the constant analyzer energy mode (29.35 eV pass energy). Charging compensation was applied assuming that C 1*s* peak appears at a binding energy of 284.8 eV. The atomic composition of the untreated and ablated samples was automatically calculated from the peak areas of the high resolution C 1*s*, O 1*s*, and N 1*s* spectra by MultiPak Spectrum V6.0A software (Physical Electronics Inc., Eden Prairie, MN) To eliminate experimental errors, the chemical composition for each sample is an average value for five points selected from the ablated surface. The C 1*s*, O 1*s*, and N 1*s* envelopes were fitted using the same software. According to the UV-laser-induced decomposition scheme established by Ortelli,[19] the C 1*s* spectra were fitted by six components related to different bonding groups, whose full width at half-maximum (FWHM) and peak position are listed in Table I. The ablation depth dependent on the laser fluence was measured with AFM (Digital Instruments, Santa Barbara, CA) (in the linear region) and a Talysurf profilometry (Rank Taylor Hobson Ltd., Leicester, United Kingdom) (in the nonlinear region).

III. RESULTS

Laser ablation of Kapton films using a frequency-tripled pulsed Nd:YAG laser at 355 nm was carried out in a single shot in a punch pattern in air, and the ablation depth was measured by AFM and a profilometer. The curve of the ablation depth as a function of the laser

fluence is shown in Fig. 2. It clearly reveals two different areas: near the ablation threshold (a linear region: 0.1–1.5 Jcm^{-2}), the ablation depth depends linearly on logarithm of the laser fluence with a slope close to the prediction by Beer's law; at higher fluences (a non-linear region, >2 Jcm^{-2}), the ablation depth deviates from Beer's law due to the effect of the photothermal ablation. The linear fit in Fig. 2 yields an effective absorption coefficient α of $(1.25 \pm 0.1) \times 10^4$ cm^{-1} and an ablation threshold F_{th} of 0.25 ± 0.02 Jcm^{-2}, while the absorption coefficient and ablation threshold at 355 nm were 2×10^4 cm^{-1} and 0.1 Jcm^{-2}, respectively.[13] This clearly indicates that the ablation mechanism is dominant for the photochemical ablation near the ablation threshold.

At higher fluences (>2 Jcm^{-2}), the carbon content on the ablated surface is markedly larger than that of the untreated sample while the oxygen content is smaller due to the photothermal decomposition and carbonization of the irradiated polymers,[17,22,25] but the reverse is true near the ablation threshold (0.34 Jcm^{-2}), as shown in Fig. 3. This clearly indicates that the residue on the ablated surface is not carbon-rich near the ablation threshold. Ortelli found that UV-laser-induced decomposition of Kapton film could be divided into two steps: the photolysis of the imide rings and ether groups and the pyrolysis of the aromatic system (carbonization).[19] After near-threshold UV laser ablation of Kapton film, a decrease of the carbon content suggests that the carbonization step may not occur due to the low surface temperature; i.e., only photolysis step takes place. On the other hand, the free radical groups from the photolysis are oxidized in air to stabilize, resulting in an increase of the oxygen content and a decrease of the carbon content. Figure 3 also shows that with an increase of the pulse number, the carbon and nitrogen contents decrease while the oxygen content increases. This suggests that further irradiation may enhance both photolysis of Kapton film and oxidation reactions of the free radical groups. To further confirm the difference of the chemical compositions at 0.34 Jcm^{-2} (near the ablation threshold) and at higher fluence, additional laser ablation was performed at 3.18 Jcm^{-2} and ten pulses when the other conditions were the same. XPS analysis shows that the carbon, oxygen, and nitrogen contents are 85.6, 11.6, and 2.8 at.%, respectively. Compared to these of the unablated sample (Table I), there is an increase of about 11 at.% for the carbon content and a decrease of approximately 7 at.%

TABLE I. Results of the peak separation of XPS C 1*s* spectra, together with the binding energy and the peak areas of C 1*s* spectra on the ablated surface.

	C–C C–H (FWHM 1.16–1.35)		C–C C–N (FWHM 0.93 eV)		C–O (FWHM 0.95 eV)		Amide (FWHM 1.00 eV)		C=O (FWHM 1.19 eV)		>C=O Phenyl shake up (FWHM 2.42 eV)	
Pulse	Peak (eV)	Area (%)	Peak (eV)	Area (%)	Peak (eV)	Area (%)	Peak (eV)	Area (%)	Peak (eV)	Area (%)	Peak (eV)	Area (%)
unablated	284.7[b]	42.8	285.6	27.2	286.3	13.47	···	···	288.6	13.5	290.9	3.07
10	284.5[b]	38.2	285.4	27.4	286.3	10.09	287.3	4.18	288.5	12.7	290.4	6.75
32	284.6[b]	41.9	285.4	21.3	286.3	11.01	287.3	8.27	288.5	11.1	290.4	6.48
100	284.6[c]	52.8	285.5	11.8	286.3	11.03	287.3	8.51	288.5	10.6	289.8	5.30
316	284.6[c]	49.6	285.5	11.8	286.3	12.6	287.3	10.22	288.5	9.77	289.8	5.91
1000	284.6[c]	44.4	285.4	15.4	286.3	15.6	287.3	9.54	288.5	9.17	289.8	5.94
3.18 × 10[a]	284.7[b]	48.3	285.4	22.7	286.3	10.15	287.1	7.12	288.3	3.76	289.8	7.93

[a]Kapton film was irradiated at a high fluence of 3.18 Jcm^{-2} and 10 pulses (in the nonlinear region).
[b]FWHM is 1.16 eV.
[c]1.35 eV.

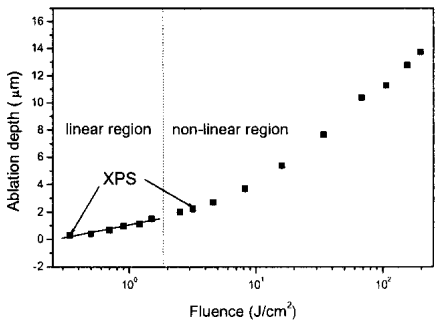

FIG. 2. Dependencies of the ablation rate on the laser fluence for the pulsed 355-nm Nd:YAG laser irradiation of Kapton film. Arrows mark the applied fluences for the XPS analysis.

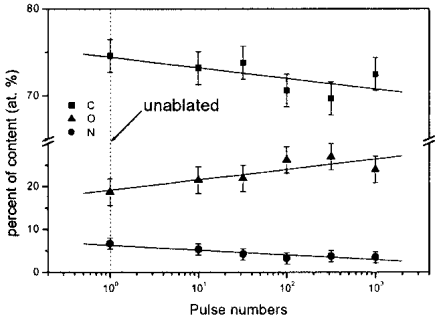

FIG. 3. Dependencies of the composition on the pulse number at 0.34 Jcm^{-2}.

for the oxygen content. This clearly indicates that the change of the carbon and oxygen contents near the ablation threshold is opposite that at higher fluence, although the decreasing nitrogen contents follow similar trends.

Figure 4 presents high-resolution XPS spectra for the C 1*s*, O 1*s*, and N 1*s* obtained from the ablated samples under different laser parameters as well as the untreated sample, clearly indicating that the peak positions and shapes are altered after laser irradiation. As shown from Fig. 4(a), the peaks of C 1*s* spectra near the threshold show a broad main peak at 284.8 eV and a chemically shifted peak at approximately 288.6 eV corresponding to the carbonyl group (C=O) in imide rings.[34] With an increase of the pulse number, the shoulder at 288.6 eV decreases gradually but does not disappear until 1000 pulses. Moreover, after UV laser ablation at 0.34 Jcm^{-2}, the peak positions for O 1*s* make an obvious shift to high binding energy [Fig. 4(b)], and the symmetry for N 1*s* is broken [Fig. 4(c)] due to the breakage of the imide rings of Kapton film and the formation of the amide groups.[17,19,22,25]

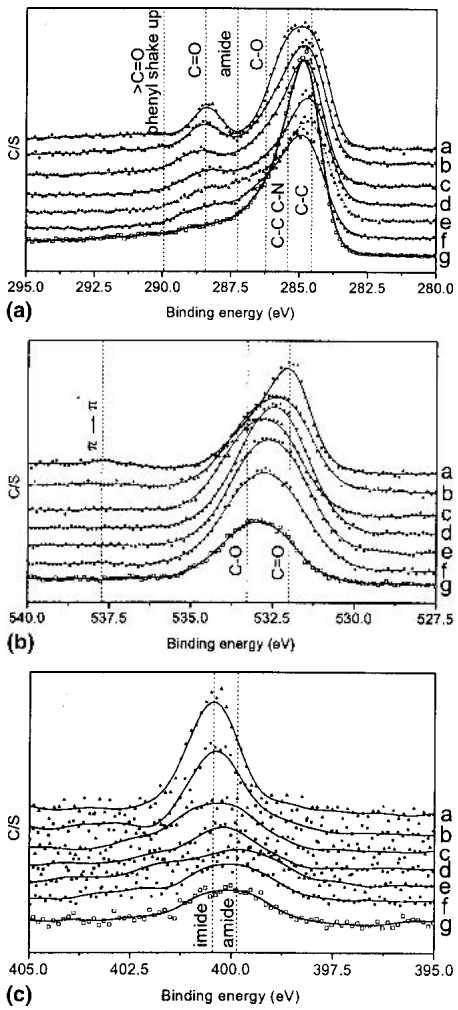

FIG.4. XPS spectra obtained from the ablated surface with different pulses and fluences: (a) C 1*s*, (b) O 1*s*, (c) N 1*s*. [(a) unablated, (b) 10 pulses, (c) 32 pulses, (d) 100 pulses, (e) 316 pulses, (f) 1000 pulses, (g) 3.18 Jcm^{-2}, 10 pulses].

As reported earlier,[24,35] for the untreated Kapton film, at least four different carbon environments are found for the C 1s region: (i) carbon atoms bonds from the aromatic rings that are not directly attached to the imide ring at 284.6 eV (C–C), (ii) carbon atoms bonded to nitrogen at 285.6 eV (C–N), (iii) carbon atoms bonded to oxygen related to the ether group (C–O), and (iv) carbon atoms bonded with oxygen in the imide ring at 288.6 eV assigned to the carbonyl group (C=O). In addition, there is a shakeup at 290.9 eV arising from the aromatic rings.[35] For the O 1*s* region, two components are detected at 532.0 eV and 533.3 eV, arising from the carbonyl group (C=O) in the imide systems and the ether group (C–O), respectively. Similar to the C 1*s* spectrum, there exists a shakeup at 537.6 eV arising from the carbonyl groups. Only 1 symmetric peak at 400.4 eV (C–N) was found for the N 1*s* region. Figure 5 displays the fitted XPS spectra of C 1*s*, O 1*s* and N 1*s*, at 0.34 Jcm^{-2} and 1000 pulses. Compared to those of the untreated sample, a new component appears at 287.4 eV for the C 1*s*, as well as at 398.8 eV for the N 1s region, related to the amide groups resulting from the breakage of the imide systems.[36] Ortelli found it as an intermediate product during the UV-laser-induced decomposition of Kapton film.[19] The non-imide carbonyl groups detected at 531.6 eV [Fig. 5(b)] further confirm the breakage of the imide groups.

To further analyze the changes of the chemical states near the threshold, a semiquantitative analysis was performed. The FWHM value for each component was fixed except for the C–C bond as shown in Table I. The peak areas of several groups for the C 1*s* were plotted versus the pulse number as shown in Fig. 6. With increasing pulse number, the content of the amide group increases, whereas the content of the carbonyl group (C=O) decreases. This is attributed to more breakage of the imide rings due to an increase of the photons absorbed for each position. According to the laser-induced decomposition path of Kapton established by Ortelli,[19] the decreasing content of the C=O group accompanies the similar change in the content of the C–O group due to the simultaneous breakage of the diaryl ether groups. However, in this case, the content of the C–O group increases with the pulse number, and at 1000 pulses is finally higher than that of the untreated sample (Fig. 6). This abnormal phenomenon may be related to the inhomogeneities in the beam profile (Gaussian mode) and the cumulative heating discussed in Sec. IV. Also, as shown in Table I, the component at 290.9 eV, corresponding to the shakeup, makes a shift to a lower binding energy of 289.8 eV assigned to the >C=O group due to the oxidation of the unstable free radical groups[25,33] after laser irradiation.

At higher fluence (3.18 J/cm^{-2}), the shoulder at 288.6 eV related to the carbonyl group disappears [Fig. 4(a)] and its peak area (3.76 at.%) is much lower than that (about 10 at.%) near the ablation threshold due to the elimination of the carbonyl groups (carbonization) as evidenced in Refs.18 and 20. Similar to difference of the surface structure,[30–32] the difference of the chemical states near the ablation threshold and at higher fluence is probably caused by the different ablation mechanisms.

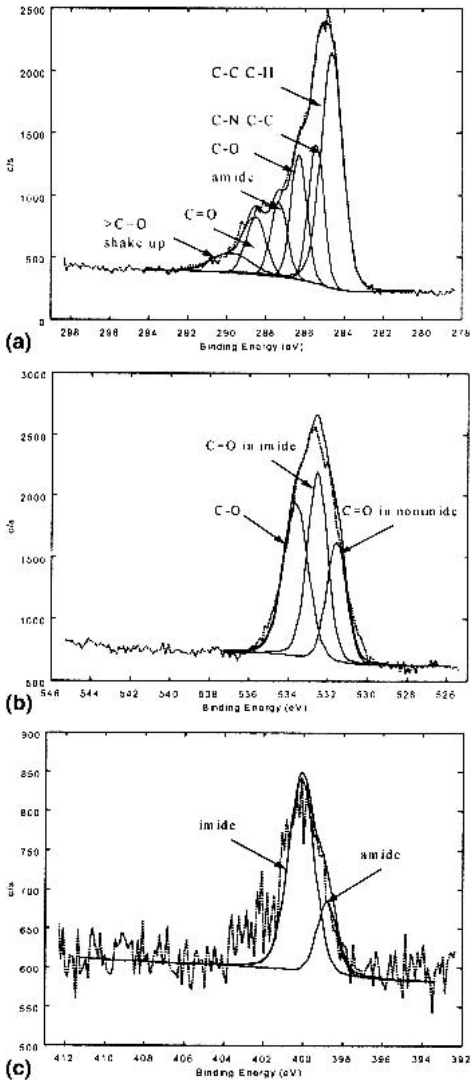

FIG. 5. Curved-fitted high-resolution XPS spectra for the ablated surface at 0.34 Jcm^{-2} and 1000 pulses: (a) C 1*s*, (b) O 1*s*, (c) N 1*s*.

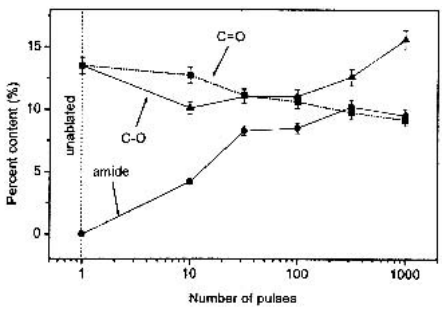

FIG. 6. Changes in the peak areas of C 1*s* spectra as a function of the pulse number for the following bonds: C=O (■), C–O (▲), and amide (●).

IV. DISCUSSION

As mentioned above, the changes of the chemical composition and characteristics near the ablation threshold are completely different than those at higher fluences (in the non-linear region). Upon further irradiation at 0.34 Jcm^{-2}, the increasing content of the amide groups and C–O groups is detected as well as the increasing oxygen content, whereas the content of the carbonyl groups slightly decreases. Investigation of these changes should be beneficial for ascertaining the UV laser ablation mechanism.

Ortelli developed a possible UV laser induced decomposition pathway of Kapton film, consisting of the photolysis and pyrolysis steps.[19] The first step is probably photon-induced decomposition of the C–N bond in the imide ring and the diaryl ether group, and then the amide group is formed as an intermediate product.[17,19] The next step is the photothermal decomposition of the aromatic systems resulting in the formation of the carbon-rich residue on the ablated surface.[19,25] In this case, since the photon energy of 355-nm Nd:YAG laser (3.48 eV) is higher than the disassociation energy of the C–N bond (3.04 eV),[37] the C–N bond in the imide rings can also be directly dissociated via photolysis, resulting in the formation of the amide groups and free radical groups. Meanwhile, a temperature rise on the ablated surface, which will take place during the laser irradiation and strongly depends on the laser fluence, can improve the efficiency of the photolysis reaction. On the other hand, unlike the UV laser ablation at higher fluence, the temperature rise cannot reach several thousand degrees centigrade (a start carbonization temperature),[38,39] which is necessary for the pyrolysis of the aromatic system, and the carbonization step cannot take place near the ablation threshold. This is substantiated by the high content of the amide groups (Table I) and no existence of the carbon-rich residue on the ablated surface (Figs. 3 and 6).

The disassociation energy of the C_{aryl}–C bond is 3.62 eV,[37] and it can be photochemically broken by the XeCl excimer laser emitting at 308 nm (the photon energy 4.02 eV),[19] but it cannot be directly disassociated by the 355-nm Nd:YAG laser (3.48 eV). We know that the Gaussian profile of the laser beam could lead to the inhomogeneous temperature profile, and the temperature rise at the center is usually much higher than that at the edge. It is believed that for the near-threshold UV

ablation, a small portion of the C_{aryl}–C bonds is thermally induced decomposed at the center where a high temperature (still less than the start carbonization temperature) is experienced, resulting in the loss of the ablation fragments such as $–C_6H_4N(CO)–$ and the decrease of both nitrogen content and the content of the carbonyl groups (Table I). The $–C_6H_4N(CO)–$ fragments off the ablated surface may continuously absorb the photons, and secondary decomposition may occur into various volatile species such as CO, CN, and C_2H_2, identified by mass spectrometry.[19] Therefore, the following decomposition pathway for the near-threshold UV laser ablation of Kapton film is presented in Fig. 7. This clearly indicates that the photochemical mechanism plays an important role during the UV pulsed Nd:YAG laser ablation of Kapton film, as suggested previously.[19,24,27] Moreover, upon further irradiation (increasing the pulse number), the creation of the amide groups is beyond their decomposition and their content continuously increases with a simultaneous decrease of the carbonyl groups (Fig. 6).

At higher fluences, the carbon-rich residue on the ablated surface produced via the carbonization of the aromatic system is considerably stable. [18] For example, the graphite materials are detected using Raman spectroscopy on the ablated surface after the laser irradiation at 308 nm.[21] In contrast, near the ablation threshold, the nitrogen-poor residue contains many unstable free radical groups (Fig. 7) and sequentially needs to become stable quickly via the oxidation reaction. On the basis of the possible decomposition pathway, two possible oxidizing reactions are presented in Fig. 8. One is that the free radicals C_{aryl}–(CO)– may undergo an oxidation to form a stable structure including the >C=O groups [Fig. 8(a)], which are detected at 289.8 eV for the C 1*s* spectra (Fig. 5). The other is the formation of the

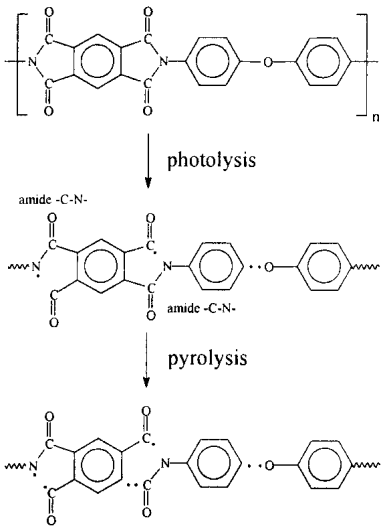

FIG. 7. Possible scheme of the decomposition of Kapton film near ablation threshold (• indicates a broken bond).[19]

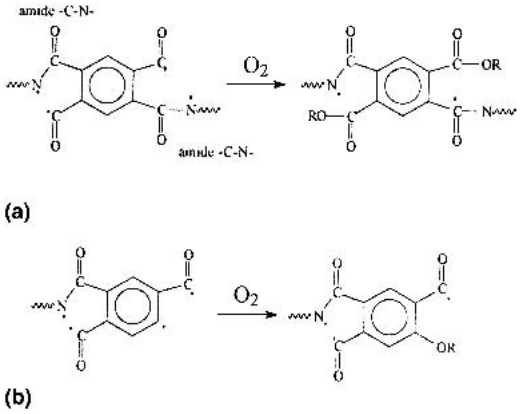

FIG. 8. Possible oxidation reactions for the unstable free radials: (a) formation of the >C=O groups, (b) formation of the C–O groups.

stable structure containing the C–O groups, as shown in Fig. 8(b). The oxidation of the free radical groups from the decomposition of Kapton film may explain the apparent discrepancy in the increase of the oxygen content as well as the decrease of the carbon content.

Finally, it is worth noting that the content of the C–O group of the ablated surface increases upon further irradiation at 0.34 Jcm^{-2} (Fig. 6). The content of the C–O group depends on two opposite factors: the thermally induced breakage of the ether groups and the disassociation of the C_{aryl}–C groups [Fig. 8(b)]. The former decreases it, but the latter increases it via oxidation of the unstable free groups. As mentioned earlier, the pyrolysis of the C_{aryl}–C groups may only take place at the center with a high temperature. At a lower pulse number, the temperature rise at the center is so low that the pyrolysis of the C_{aryl}–C groups is still difficult, but the lower temperature rise may induce the photolysis of the diaryl ether groups. Thus, the content of the C–O group is lower than that of the untreated samples at a lower pulse number (Fig. 6). However, at higher pulse number (1000 pulses), the higher temperature rise caused by the cumulative heating[40] leads to more breakage of the C_{aryl}–C groups although the diaryl ether groups are simultaneously broken. When the breakage of the C_{aryl}–C groups is beyond the disassociation of the diaryl ether groups, the content of the C–O group may be higher than that of the untreated sample (Fig. 6). Therefore, the cumulative heating can induce the disassociation of the C_{aryl}–C groups and enhance the oxidation reaction of the unstable free radical groups, producing an increase of the stable species including the C–O groups with an increase in the pulse number.

V. CONCLUSIONS

Near-threshold (0.34 Jcm^{-2}) UV laser ablation of Kapton film was carried out using a pulsed Nd:YAG laser emitting at 355 nm. The changes of the chemical composition and characteristics on the ablated surface of

Kapton film were measured by the surface-sensitive XPS technique. In near-threshold UV laser ablation, different from irradiation at higher fluences, the pyrolysis of the aromatic system may not occur due to a low surface temperature rise; i.e., only photolysis of the C-N bond in the imide rings and the ether group (C-O) takes place, producing the amide structure and many unstable free radical groups. Sequentially, the oxidation reaction occurs to stabilize the free radical groups and the >C=O groups are generated. The changes in the chemical composition and characteristics are quite compatible with the decomposable mechanism. Upon further irradiation, the cumulative heating may induce the breakage of the C_{aryl}–C bond and enhance the oxidation reaction, and then the C–O group content increases.

ACKNOWLEDGMENT

Financial support from the Open Foundation of the State Key Laboratory of Plastic Forming Simulation and Mould Technology is gratefully acknowledged.

REFERENCES

1. R. Srinivasan and V. Mayne-Banton, Appl. Phys. Lett. **40,** 40 (1982).
2. E. Andrew, P.E. Dyer, D. Forster, and P.E. Key, Appl. Phys. Lett. **43,** 717 (1983).
3. A. Beuhler, A. Tungare, and J. Savic, Circuit World **24,** 36 (1998).
4. J.H. Brannon, J.R. Lankard, A.I. Baise, F. Burns, and J. Kaufman, J. Appl. Phys. **58,** 2036 (1985).
5. S.R. Cain, J. Phys. Chem. **97,** 7572 (1993).
6. G.B. Blanchet, C.R. Fincher, Jr., C.L. Jackson, S.I. Shah, and K.H. Gardner, Science **262,** 719 (1993).
7. H. Fukumura, K. Hamano, and H. Masuhara, J. Phys. Chem. **97,** 12110 (1993).
8. X. Wen, D.E. Hare, and D.D. Dlott, Appl. Phys. Lett. **64,** 184 (1994).
9. B.J. Plamer, T. Keyes, R.H. Clarke, and J.M. Isner, J. Phys. Chem. **93,** 7509 (1989).
10. H.H.G. Jellinek and R. Srinivasan, J. Phys. Chem. **88,** 3048 (1984).
11. R. Srinivasan, J. Appl. Phys. **72,** 1651 (1992).
12. R. Srinivasan, Appl. Phys. A **56,** 417 (1993).
13. Winco K.C. Yung, J.S. Liu, H.C. Man, and T.M. Yue, J. Mater. Process. Tech. **101,** 306 (2000).
14. T. Lippert, J. Stebani, J. Ihlemann, O. Nuyken, A. Wokaun, and R. Srinivasan, J. Phys. Chem. **97,** 12296 (1993).
15. P.E. Dyer, G.A. Oldershaw, and D. Schudel, J. Phys. D: Appl. Phys. **25,** 323 (1992).
16. J.H. Brannon, D. Scholl, and E. Kay, Appl. Phys. A **52,** 160 (1991).
17. K.C. Yung and D.W. Zeng, Surf. Coat. Technol. **145,** 186 (2001).
18. R. Srinivasan, R.R. Hall, W.D. Loehle, W.D. Wilson, and D.C. Allbee, J. Appl. Phys. **78,** 4881 (1995).
19. E.E. Ortelli, F. Geiger, T. Lippert, J. Wei, and A. Wokaun, Macromolecules **33,** 5090 (2000).
20. E.E. Ortelli, F. Geiger, T. Lippert, and A. Wokaun, Appl. Spectrosc. **55,** 412 (2001).
21. T. Lippert, E. Ortelli, J.C. Panitz, F. Raimondi, J. Wambach, J. Wei, and A. Wokaun, Appl. Phys. A **69,** s651 (2000).
22. B. Schnyder, J. Wambach, Th. Kunz, Ch. Hahn, and R. Kotz, J. Electron. Spectrosc. **105,** 113 (1999).
23. D.A. Wesner, M. Aden, J. Gottmann, A. Husmann, and E.W. Kreutz, Fresenius J. Anal. Chem. **365,** 183 (1999).
24. D.W. Zeng, K.C. Yung, and C.S. Xie, Surf. Coat. Technol. **153,** 210 (2002).
25. K.C. Yung, D.W. Zeng, and T.M. Yue, Appl. Surf. Sci. **173,** 193 (2001).
26. D.W. Zeng and K.C. Yung, Appl. Surf. Sci. **180,** 280 (2001).
27. S. Küper, J. Brannon, and K. Brannon, Appl. Phys. A **56,** 43 (1993).
28. B. Luk'yanchuk, N. Bityurin, S. Anisimov, N. Arnold, and D. Bäuerle, Appl. Phys. A **62,** 397 (1996).
29. B. Luk'yanchuk, N. Bityurin, M. Himmelbauer, N. Arnold, and D. Bäuerle, Nucl. Instrum. Methods Phys. Res. B **122,** 347 (1997).
30. M. Himmelbauer, E. Arenholz, D. Bäuerle, and K. Schilcher, Appl. Phys. A **63,** 337 (1996).
31. M. Himmelbauer, N. Arnold, N. Bityurin, E. Arenholz, and D. Bäuerle, Appl. Phys. A **64,** 451 (1996).
32. D. Bäuerle, M. Himmelbauer, and E. Arenholz, J. Photochem. Photobio. A: Chem. **106,** 27 (1997).
33. M.K. Ghosh and K.L. Mittal, *Polyimides: Fundamentals and Applications* (Marcel Dekker, New York, 1996), p. 222.
34. L.J. Matienzo and F.D. Egitto, Polym. Degrad. Stabil. **35,** 181 (1992).
35. G. Beamson and D. Briggs, *High Resolution XPS of Organic Polymers: The Scienta ESCA300 database* (John Wiley & Sons, New York, 1992), p. 214.
36. J.T. Wolan and G.B. Hoflund, J. Vac. Sci. Technol. A **17,** 662 (1999).
37. W.W. Dueley, *UV Lasers: Effects and Applications in Materials Science* (Cambridge University Press, New York, 1996), p. 150.
38. T. Takeichi, Y. Eguchi, Y. Kaburagi, Y. Hishiyama, and M. Inagaki, Carbon **37,** 569 (1999).
39. Y. Hishiyama, A. Yoshida, and M. Inagaki, Carbon **36,** 1113 (1998).
40. F.C. Burns and S.R. Cain, J. Phys. D: Appl. Phys. **29,** 1349 (1996).